Journal of
Synchrotron
Radiation

ISSN 0909-0495

Received 3 September 2007
Accepted 16 January 2008

An extraction algorithm for core-level excitations in non-resonant inelastic X-ray scattering spectra

H. Sternemann,[a]* C. Sternemann,[a]* G. T. Seidler,[b] T. T. Fister,[b] A. Sakko[c] and M. Tolan[a]

[a]Fakultät Physik/DELTA, Technische Universität Dortmund, Maria-Göppert-Mayer-Strasse 2, D-44221 Dortmund, Germany, [b]Physics Department, University of Washington, Seattle, USA, and [c]Department of Physical Sciences, University of Helsinki, Helsinki, Finland.
E-mail: henning.sternemann@uni-dortmund.de, christian.sternemann@uni-dortmund.de

Non-resonant inelastic X-ray scattering of core electrons is a prominent tool for studying site-selective, *i.e.* momentum-transfer-dependent, shallow absorption edges of liquids and samples under extreme conditions. A bottleneck of the analysis of such spectra is the appropriate subtraction of the underlying background owing to valence and core electron excitations. This background exhibits a strong momentum-transfer dependence ranging from plasmon and particle–hole pair excitations to Compton scattering of core and valence electrons. In this work an algorithm to extract the absorption edges of interest from the superimposed background for a wide range of momentum transfers is presented and discussed for two examples, silicon and the compound silicondioxide.

Keywords: non-resonant inelastic X-ray scattering; core-level excitations; Compton scattering; X-ray absorption; silicon.

1. Introduction

Non-resonant inelastic X-ray scattering (NRIXS) of core electrons, often referred to as X-ray Raman scattering (XRS), is a unique tool for accessing shallow absorption edges with high-energy X-rays [a comprehensive overview on the history of NRIXS and its recent developments is given by Schülke (2007)]. Hence, it is an important technique with a growing rate of applications for studying bulk properties (Balasubramanian *et al.*, 2007; Sternemann, Sternemann *et al.*, 2007; Mattila *et al.*, 2005; Sternemann, Soininen *et al.*, 2005; Bergmann *et al.*, 2002), liquids (Bergmann *et al.*, 2007; Cai *et al.*, 2005; Wernet *et al.*, 2004) or systems in extreme environments (Kumar *et al.*, 2007; Lee *et al.*, 2007; Mao *et al.*, 2006; Arms *et al.*, 2005) where soft X-rays or electrons cannot be used as a probe. Because NRIXS is a scattering process, a finite momentum transfer q according to the scattering angle φ is employed. Thus, the selection rules for excitation channels can be chosen freely and final states of different orbital momentum can be studied (Feng *et al.*, 2004; Sternemann *et al.*, 2003; Hämäläinen *et al.*, 2002). Soininen *et al.* (2006) showed that the projected unoccupied density of states is accessible with q-dependent NRIXS. Recently, the background proportional enhancement of the extended fine structure in NRIXS by variation of the momentum transfer was demonstrated (Fister, Seidler, Hamner *et al.*, 2006). Therefore, employing the q-dependence of NRIXS is of significant importance in such studies. With the advent of synchrotron radiation the applications of NRIXS spectroscopy strongly increased and, during recent years, various experimental set-ups have become accessible at third-generation synchrotron sources. *Inter alia* these are spectrometers at beamline ID16 of the European Synchrotron Radiation Facility (Krisch *et al.*, 1997), the Taiwan beamline BL12XU of SPring-8 (Cai *et al.*, 2004), and the beamlines 13-IDD (Meng *et al.*, 2004; Mao *et al.*, 2003), 16-IDD (Kumar *et al.*, 2007), 18-IDD (Bergmann & Cramer, 1998) and 20-ID (Fister, Seidler, Wharton *et al.*, 2006) of the Advanced Photon Source (APS).

Whereas the experimental set-ups for q-dependent NRIXS studies have become very sophisticated by using multiple analyzers in vertical scattering geometry or multiple analyzer arrays in horizontal scattering geometry, the extraction of the data is still a challenge. This is due to the fact that the core excitations of interest are usually superimposed by contributions of valence electrons or other core electrons. Therefore, we present in this article an algorithm for the modeling and subtraction of the scattering background to extract the relevant core excitation spectrum. It is applicable to various samples because no theoretical calculations apart from tabulated Hartree–Fock core-electron Compton profiles (Biggs *et al.*, 1975) are required. The algorithm is illustrated by an extraction of the Si L edges in pure Si and the compound SiO_2 from a multiple-q NRIXS experiment conducted at beamline XOR/PNC 20-ID of APS.

The layout of the paper is as follows. In §2 the experimental set-up is described briefly. The energy-dependent cross-

section corrections, the experimental determination of the valence electron contribution and the extraction of the Si L edges are presented and exemplified for Si and SiO_2 in §3. Furthermore, the obtained Si L edges of Si and SiO_2 are compared with q-dependent calculations. Finally, a summary and a short outlook are given.

2. Experiment

The experiment has been performed at beamline XOR/PNC 20-ID of APS employing the LERIX set-up for a simultaneous acquisition of NRIXS spectra for multiple momentum transfers. A detailed overview on this spectrometer is given by Fister, Seidler, Wharton *et al.* (2006). In the actual stage of expansion, 19 Si(555) analyzers are arranged on a semicircle of radius 1 m with scattering angles between 9° and 171°. The Rowland-circle plane is perpendicular to the polarization of the X-ray beam so that the measured intensity is independent with respect to the polarization factor. The experiment has been performed in inverse geometry, *i.e.* the incoming photon energy was tuned with a fixed analyzer energy at 9.893 keV with a spread of 0.16 eV for the different analyzer crystals. With the Si(111) double-crystal monochromator an energy resolution of 1.5 eV could be obtained. The Si and SiO_2 powder samples have been pressed into pellets and aligned to the center of the analyzer circle. The incident angle has been set to $\varphi_i = 10°$ in reflection geometry. Thus, the first two analyzers were partly or fully shadowed by the sample so that spectra for a q-range from 1.25 a.u. to 5.34 a.u. have been recorded. For each sample several single scans were performed and added up subsequently to exclude systematic errors during the measurement. The added raw data of Si and SiO_2 from different detectors are shown in Fig. 1. The energy-loss positions of the Si $L_{II,III}$, Si L_I, and O K and L_I edges are indicated by vertical lines. All spectra are shifted vertically with respect to their absolute value of momentum transfer calculated for the energy-loss positions of the Si $L_{II,III}$ edges. The spectra are normalized to their peak value.

3. Extraction algorithm for core electron excitations

The measured quantity in an inelastic X-ray scattering experiment is the double differential scattering cross section (DDSCS). It can be expressed in terms of the dynamic structure factor $S(\mathbf{q},\omega)$ (natural units are used with $\hbar = c = 1$),

$$\frac{d^2\sigma}{d\Omega d\omega} = \left(\frac{d\sigma}{d\omega}\right)_{Th} \frac{\omega_2}{\omega_1} S(\mathbf{q},\omega) \quad (1)$$

$$= r_0^2 (\boldsymbol{\varepsilon}_1 \cdot \boldsymbol{\varepsilon}_2)^2 \frac{\omega_2}{\omega_1} S(\mathbf{q},\omega). \quad (2)$$

The coupling of the X-rays with the electrons of the system is described by the Thomson scattering cross section, $(d\sigma/d\omega)_{Th}$, with the classical electron radius r_0 and the polarization vector $\boldsymbol{\varepsilon}_{1/2}$ of the incoming and outgoing photon. $\omega_{1/2}$ denotes the energy of the incident and scattered photon. The momentum transfer q is defined by $q^2 = \omega_1^2 + \omega_2^2 - 2\omega_1\omega_2\cos\varphi$. The dynamic structure factor yields information about time-dependent electron density fluctuations (Schülke, 2007). In the limit of high momentum transfers the DDSCS can be expressed in terms of the so-called Compton profile, $J(p_z)$,

$$\frac{d^2\sigma}{d\Omega d\omega} = r_0^2 (\boldsymbol{\varepsilon}_1 \cdot \boldsymbol{\varepsilon}_2)^2 \frac{\omega_2}{\omega_1} \frac{m}{q} J(p_z), \quad (3)$$

with $p_z = m/q\,\omega - q/2$, the component of the scattered electron's momentum in the ground state parallel to the momentum transfer $\mathbf{q}$. Compton scattering provides access to the ground-state electron density [see *e.g.* Cooper *et al.* (2004) or Schülke (2007) for a review on Compton scattering].

Valence electron excitations manifest themselves in the dynamic structure factor and transform from the typical plasmon and particle–hole excitation spectrum for low momentum transfer to the valence electron Compton profile at high momentum transfer. A calculation of the valence electron contribution is difficult and not appropriate for an all-purpose extraction algorithm. Here a model function has to be used to approximate the shape of the underlying valence electron contribution. Within the Compton limit usually the valence Compton profile can be extracted for a certain momentum transfer value out of the experimental data. This

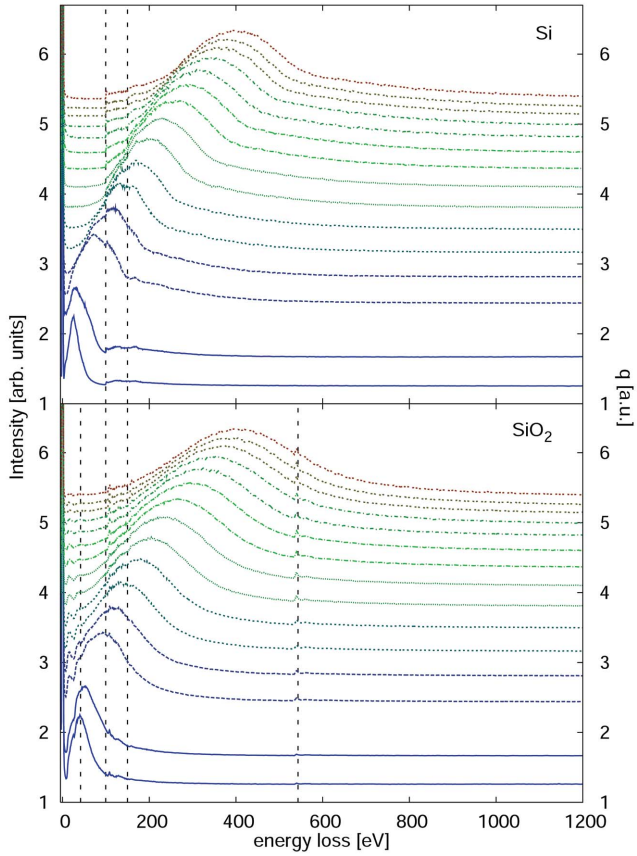

Figure 1
Raw NRIXS data of Si (top) and SiO_2 (bottom) for different momentum transfers. The spectra are shifted vertically with the axis of ordinates intercept at the according momentum transfer. For Si the Si L edges are indicated by vertical lines. For SiO_2 the positions of the O K and L_I edges are also shown. This figure is in color in the electronic version of this paper.

profile then properly reflects the valence electron contribution to the NRIXS spectrum for medium and high momentum transfers. The core electron contribution to the total NRIXS spectrum of an element or a compound is well described by its atomic Hartree–Fock Compton profiles which exist in tabulated form (Biggs *et al.*, 1975). Such profiles can be included straightforwardly into a subtraction algorithm. Nevertheless, close to an absorption edge, where the corresponding core electron contribution sets in, the spectrum is dominated by dynamical effects, the local environment of the excited atoms and by their electronic structure. Thus it shows significant deviations from the onset of a Hartree–Fock core electron Compton profile.

An algorithm scheme for the extraction of core electron contributions to the NRIXS spectrum, hence referred to as an absorption edge, was developed and will be described in the following. Before such an absorption edge can be extracted, various energy-dependent corrections have to be taken into account. In the following these corrections will be discussed, then the extraction of the valence electron Compton profile is described, followed by a detailed demonstration of the extraction of the Si $L_{\rm II,III}$ absorption edge for the measured systems Si and SiO_2.

3.1. Energy-dependent corrections

The intensity measured in the detector has to be corrected for the background scattering, energy-dependent absorption of the incoming and scattered X-rays within the sample, and absorption of the incoming X-rays by, for example, windows, foils or air paths. Moreover, a cross-section correction has to be applied. Absorption and efficiency corrections might also be necessary for the monitor detector signal. The appropriate energy-dependent corrections related to the LERIX set-up are discussed in the following.

3.1.1. Absorption and self-absorption. In reflection geometry the correction for self-absorption of the incoming and scattered X-rays within a sample of thickness d is given by

$$I_{\rm Re} \propto I_0 \, \frac{1-\exp\left[-d(\mu_{\rm i}/\cos\varphi_{\rm i}+\mu_{\rm f}/\cos\varphi_{\rm f})\right]}{\mu_{\rm i}/\cos\varphi_{\rm i}+\mu_{\rm f}/\cos\varphi_{\rm f}}, \qquad (4)$$

with the absorption length $\mu_{\rm i/f}$ for the incident and the analyzer energy, respectively. $\varphi_{\rm i/f}$ are the corresponding scattering angles relative to the normal of the sample surface. For transmission geometry the correction is

$$I_{\rm Tr} \propto I_0 \, \frac{\exp\left[-d(\mu_{\rm f}/\cos\varphi_{\rm f})\right]-\exp\left[-d(\mu_{\rm i}/\cos\varphi_{\rm i})\right]}{\mu_{\rm i}/\cos\varphi_{\rm i}-\mu_{\rm f}/\cos\varphi_{\rm f}}. \qquad (5)$$

Further absorption, *e.g.* owing to air, Be- or Kapton-windows in the beam path, can be accounted for by the simple transmission correction factor

$$I_{\rm Tr} = I_0 \exp\left(-d\mu_{\rm i/f}\right). \qquad (6)$$

This energy-dependent absorption correction has to be applied for the beam paths of the incident beam between normalization detector and sample, because only the incident energy is varied in inverse geometry and the analyzed energy is kept constant. Corrections for the normalization detector itself have to be considered separately.

3.1.2. Compton cross-section correction. For the extraction of the valence Compton contribution the experimental Compton profile $J(p_z)$ has to be calculated from the DDSCS. In the non-relativistic limit the Compton profile $J(p_z)$ is directly proportional to the DDSCS [see equation (3)]. In the relativistic case it needs to be corrected according to Ribberfors (1975) and Holm (1988)

$$\frac{{\rm d}^2\sigma}{{\rm d}\Omega{\rm d}\omega} = \frac{r_0^2}{2}\frac{\omega_2}{\omega_1}\,\chi(p_z)\,\frac{m}{q}\,J(p_z) \qquad (7)$$

by the p_z-dependent

$$\chi(p_z) = \frac{R}{R'}+\frac{R'}{R}-\sin^2\theta, \qquad (8)$$

where θ is the scattering angle and the parameters R and R' are given by

$$\begin{aligned} R &= \omega_1\left[m-(\omega_1-\omega_2\cos\theta)\frac{p_z}{q}\right], \\ R' &= R-\omega_1\omega_2(1-\cos\theta). \end{aligned} \qquad (9)$$

Fig. 2 shows the corrections owing to the Compton cross section and the self-absorption in the sample. As typical for inverse geometry, both contributions compensate in parts. Fig. 2 shows further the absorption correction owing to air and Kapton in the beam path.

3.1.3. Background. Parasitic scattering, *e.g.* from the He in the analyzer scattering path, leads to a background in the spectra which in first approximation is assumed to be constant. The detector energy resolution plays an important role in rejecting stray elastic scattering in some inelastic X-ray scattering experiments. In such cases, an additional background component reflecting the detector's energy response would be added to the present algorithm when extracting the NRIXS at low-lying edges. In the present case, however, the spatial filtering of the LERIX design reduces such stray counts to

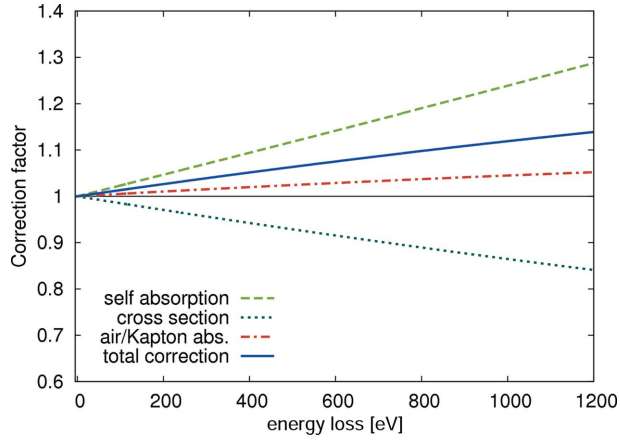

Figure 2
Absorption corrections and relativistic Compton cross section. The DDSCS has to be divided by the total correction to obtain the Compton profile $J(p_z)$. This figure is in color in the electronic version of this paper.

negligible levels despite the poor energy resolutions (∼2 keV) of the detectors (Fister, Seidler, Wharton *et al.*, 2006). For an estimation of the background level, scattering is recorded for energies below the quasi-elastic line. For energy losses far away from absorption edges in the system the Hartree–Fock Compton core profiles should match very well the experimental scattering intensity. Thus the background can be refined by adjusting the spectra to the calculation in that energy regime.

3.2. Extraction of the valence electron Compton profile

The contribution of core electrons to the Compton profile can be well approximated by atomic Hartree–Fock calculations. However, to model the valence electron contributions adequately, more sophisticated calculations have to be used as discussed earlier. Nevertheless, this contribution can also be extracted from the experimental spectra if, at a certain momentum transfer, the valence regime is not covered by an absorption edge. This should be possible for multi-q data sets as obtained with the LERIX set-up. Fig. 3 shows the spectra of Si and SiO_2 for a momentum transfer of $q = 5.21$ a.u. where the energy range of the valence contribution extends beyond the onset of the Si L absorption edges. For the separation of the valence profile from the core signal of the Si L edges (and the O K edge for SiO_2) an adequate description of the latter contribution is necessary. In the following, a scheme for the modeling of the core profile including its asymmetry will be discussed. Furthermore, the valence contribution also shows an asymmetry which has to be taken into account for the final extraction of the NRIXS signal.

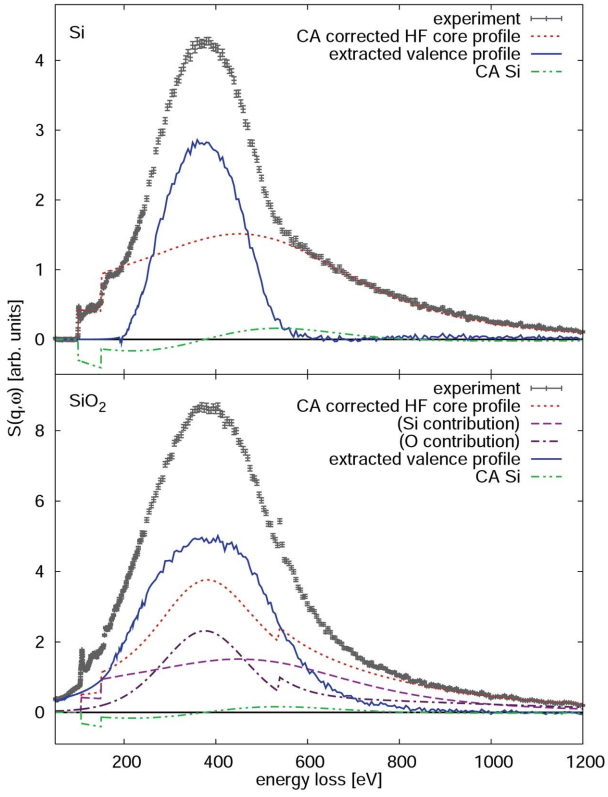

Figure 3
Extraction of the valence contribution to the Compton profile for Si (top) and SiO_2 (bottom) at $q = 5.21$ a.u. The asymmetry-corrected Hartree–Fock (HF) core contributions for Si and O are shown separately. For Si the correction to the nonrelativistic Compton cross section (CA) is taken into account. The experimental spectra and the core profiles are normalized to the according number of electrons. This figure is in color in the electronic version of this paper.

The core contributions of the Si L shell have been modeled by corrected Hartree–Fock calculations. The non-relativistic Compton cross section in impulse approximation is a symmetric function in p_z space with its maximum at $p_z = 0$. However, Holm & Ribberfors (1989) have calculated the first corrections to the non-relativistic Compton cross section for the 1s, 2s and 2p shells showing asymmetries in terms of p_z. Widths and strengths of the corrections $J_1^{1s}(p_z)$, $J_1^{2s}(p_z)$ and $J_1^{2p}(p_z)$ [Holm & Ribberfors, 1989; equations (54) and (55)] have been normalized by comparing the maximum of the non-relativistic expression [Holm & Ribberfors, 1989; equations (51) and (52)] with the maximum of the Hartree–Fock profile of the according shell. The q-dependent core asymmetry corrections (CA) for Si are then added to the symmetric Hartree–Fock profiles. The corrected core profile for Si shown in the top part of Fig. 3 shows good agreement both at the onset of the Si L edges and for an energy loss beyond 600 eV where the valence contribution has vanished. However, the asymmetry correction calculated by Holm & Ribberfors (1989) can lead to deviations in magnitude and overall shape between experiment and the model for the core profile. Thus, within the presented extraction scheme a scaling factor can be applied to the core asymmetry to yield better agreement with the experiment. In the case of Si and SiO_2 a value of 1.5 is used. More sophisticated theories for the core asymmetries, as presented by Huotari *et al.* (2001), yield a better description but are not suitable to be used in a straightforward extraction algorithm. For samples where simple asymmetry theories fail to describe the experimental observation, the core asymmetry can also be directly extracted from the experiment and parametrized by a phenomenological function. The question of q-dependence of such an *ad hoc* extraction then remains unanswered. After normalization of the experimental spectrum and the core contribution to the appropriate number of electrons in p_z space, the valence contribution of the Compton profile can be extracted from the spectrum without free parameters apart from the constant background. Artefacts in the tail of the extracted valence profile owing to the onset of the Si L edges can be smoothly removed by fitting a Pearson function [see equation (11)] in this energy regime. For SiO_2 the core contribution consists of the Si and O L edges. Thus, eight O and six Si valence electrons contribute to the SiO_2 valence Compton profile. The valence profiles are then symmetrized with respect to $p_z = 0$ and smoothed by convolution with a Gaussian function. By employing the definition of p_z the valence profiles can now be calculated for all momentum transfers.

The asymmetry of the valence Compton profiles (Huotari *et al.*, 2001; Sternemann *et al.*, 2000) are modeled in p_z space by the phenomenological function (α_n: fitting parameters)

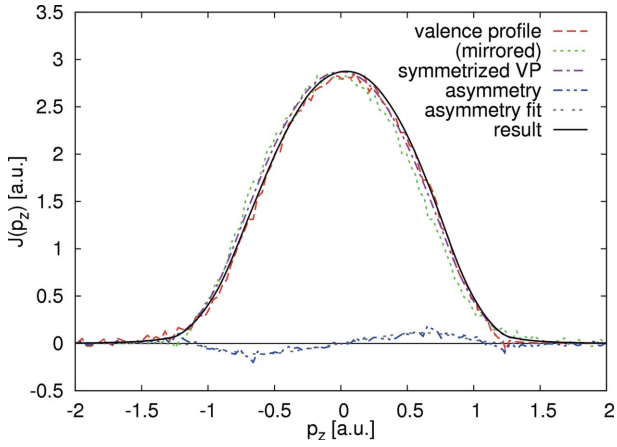

Figure 4
Determination of the asymmetry of the valence contribution to the Compton profile by mirroring of the profile at $p_z = 0$. The asymmetry is modeled as explained in the text; the resulting sum of the symmetrized valence profile and the modeled asymmetry shows good agreement with the original profile. This figure is in color in the electronic version of this paper.

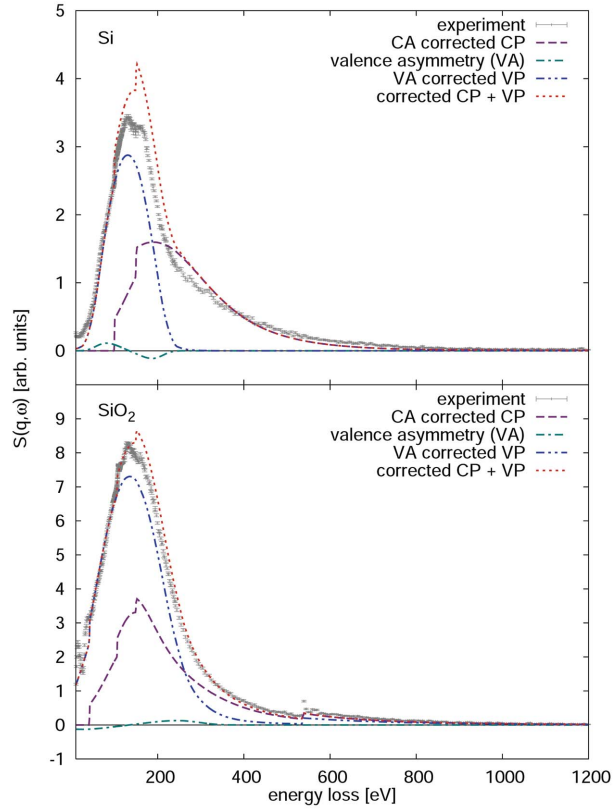

Figure 5
Extraction of the Si L edges in Si (top) and SiO_2 (bottom) for $q = 3.15$ a.u. by subtraction of the valence asymmetry (VA) corrected valence profile (VP). The sum of the core and valence contributions show good qualitative agreement in the case of SiO_2 and sufficient agreement in the case of Si with the experiment, though in the near-edge region the HF profiles are significantly larger than the experiment. For SiO_2 the offset between the valence profile and the intensity of the experiment before the edge onset can be attributed to EXAFS-like oscillations of the O L_I edge. This figure is in color in the electronic version of this paper.

$$A(p_z) = \alpha_1 \tanh\left(p_z/\alpha_2\right) \exp\left[-\left(p_z/\alpha_3\right)^4\right] \qquad (10)$$

as shown in Fig. 4 for Si. In a first approximation this asymmetry is assumed to be independent of the momentum transfer and added to the symmetrized valence contributions for all q. A q-dependent asymmetry of the valence profile is out of scope of this data treatment. The asymmetry-corrected valence profiles which are obtained from the extraction algorithm can now be used to discriminate the pure NRIXS spectrum of the Si L edges from the experimental spectra.

3.3. Extraction of the Si $L_{II,III}$ edges

In the following, the extraction of the absorption edges of interest from the q-dependent total signal will be discussed separately for high and intermediate momentum transfers and for low momentum transfers. Finally, the quality of the resulting spectra will be reviewed.

3.3.1. Intermediate and high momentum transfers. With the corrected valence Compton profile the absorption edges of interest can finally be discriminated from the underlying signal. The top parts of Figs. 5 and 6 show two examples for the extraction of the Si L edges in Si for an intermediate and a high momentum transfer, respectively. The spectra are selected to show both the performance and the limits of the presented algorithm. For intermediate momentum transfer

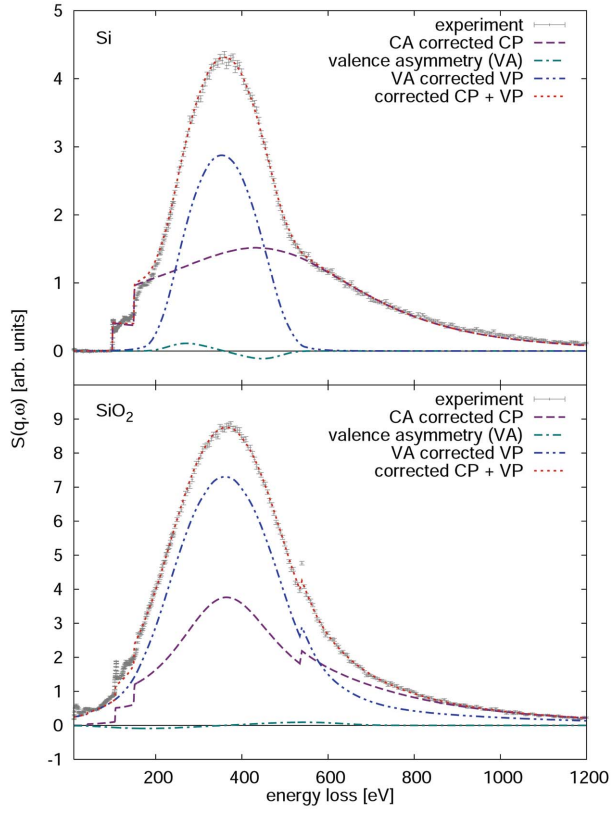

Figure 6
Extraction of the Si L edges in Si (top) and SiO_2 (bottom) for $q = 5.10$ a.u. The sum of the core and valence contributions shows very good quantitative agreement with the experiment. This figure is in color in the electronic version of this paper.

the corrected Hartree–Fock core profiles and the corrected valence profiles show adequate qualitative and quantitative agreement with the shape of the experimental spectrum on the full energy scale while it is almost perfect for high momentum transfer.

This is due to the fact that for intermediate and low q the impulse approximation is not valid. The deviations close to the edge onsets are due to the modulations of the edges which one is actually interested in. Moreover, it can be seen in Fig. 5 that the core asymmetry correction by Holm & Ribberfors (1989) cannot give a proper description for the near-edge region of the Si $L_{\rm II,III}$ edges in Si. This is not the case for SiO_2 where the O $L_{\rm I}$ edge contribution dominates the spectrum. In this procedure the constant scattering background value is refined to achieve the best agreement with the experiment. The Si L contributions can then be obtained by subtracting the corrected valence contributions from the spectra. Likewise, the extraction can be performed for the different momentum transfers. For other materials also the underlying core contributions which should not be part of the extracted spectra can in general be subtracted by the corrected Hartree–Fock profiles. The comparison of the corrected sum of valence and core contributions with the experiment exhibits a measure for the quality of the NRIXS extraction. This is strongly dependent on the relative position of the edge onset to the Compton spectrum. For the Si $L_{\rm II,III}$ edges, above q = 3.7 a.u. the onset ($\sim$100 eV) is sufficiently far away from the Compton maximum. Therefore, only the spectral weight of the full profile is affected by the background refinement and the quality of the valence profile, while the near-edge structure shows only low sensitivity. For intermediate q (2.4 a.u. $< q <$ 3.2 a.u.) the edge onset is very close to the maximum of the valence contribution. In particular, the near-edge regime of the Si $L_{\rm II,III}$ edges is rather sensitive to the shape of the valence profile and the parametrization of the valence asymmetry. For $q <$ 2.4 a.u. the subtraction of a Pearson function yields better results than the valence subtraction as will be discussed in the next paragraph. For SiO_2 (lower parts of Figs. 5 and 6) the overall agreement between the total sum of the corrected Compton profiles with the experiment is of comparable quality as for Si. However, in Fig. 5 the experimental spectrum shows modulations close to the onset of the Si $L_{\rm II,III}$ edges. They can be attributed to EXAFS-like oscillations of the O $L_{\rm I}$ edge at 41.6 eV which cannot be removed by the subtraction of the valence electron contribution. Thus, the error of the extracted NRIXS spectra is systematically and inherently increased close to the edge onset. Though beyond the scope of this article, an approach to compensate such oscillations could be a theoretical computation of the EXAFS spectrum, for instance employing the *ab initio FEFF* code (Ankudinov *et al.*, 1998; Soininen *et al.*, 2005). The valence profile and its asymmetry correction is very broad for SiO_2 since it includes the O 2p electrons. Hence, the NRIXS extraction is critical because the edge onset lies close to the Compton maximum for a wider q-range (2.4 a.u. $< q <$ 3.8 a.u.) than for Si. For the spectra with the edge onset closest to the maximum of $S(\mathbf{q},\omega)$ (2.4 a.u. $< q <$ 2.8 a.u.) the valence subtraction turned out to be insufficient. A subtraction of a Pearson function is also inadequate close to the Compton maximum, so that the two spectra in this regime were excluded from analysis. Above q = 4.2 a.u. the extraction again is very robust.

3.3.2. Small momentum transfers. For momentum transfers below 2.4 a.u. the modeled Compton profile can only poorly approximate the particle–hole excitations/plasmon spectrum. The slowly decreasing high-energy-loss tail of these contributions, which is strongly influenced by electron–electron correlation and band structure effects (Sternemann, Huotari *et al.*, 2005), cannot be modeled by simple theoretical *ab initio* approaches within the scope of an extraction scheme as presented in this work. Hence, the extraction of the Si L edges is performed by fitting a parametrized function to the region before the edge onset as shown in Fig. 7. A Pearson function was found to be a good representation for the slowly decreasing tail of the excitation spectrum for low q (β_n: fitting parameters),

$$P(\omega) = \beta_1\left[\beta_3^2(\omega - \beta_2)^2 + 1\right]^{-\beta_4}. \qquad (11)$$

Whereas the near-edge region is hardly affected by the slope of the background function, uncertainties for the absolute intensity of the extracted edges grow especially for high curvatures in the background function.

An alternative approach for the background subtraction would be the modification of the valence Compton profile with the phenomenological local field correction (LFC) factor $G(q)$ (Hubbard, 1957) in the dielectric function. The LFC factor introduces an additional asymmetry into the valence profile to model the typically increasing skewness of $S(\mathbf{q},\omega)$ for lower momentum transfer in a phenomenological way. Nonetheless, for the low-q extraction of the spectra presented in this article the Pearson method yields the better results and is therefore applied.

3.3.3. Result. For Si the extraction of the Si L edges can be performed as described in the two preceding sections for 16 different momentum transfers. For q = 2.41 a.u. the maximum

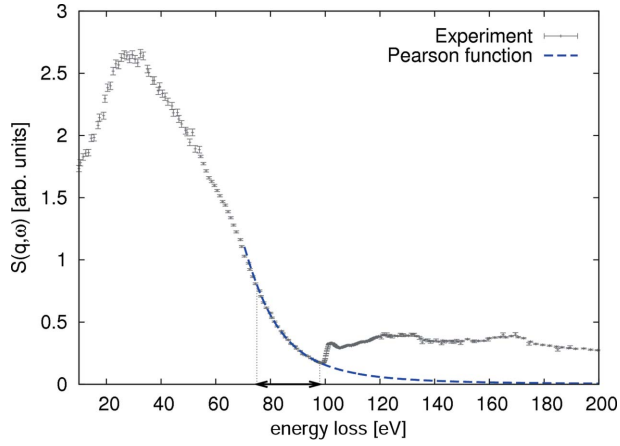

Figure 7
Extraction of Si L edges in Si for q = 1.66 a.u. by subtraction of a Pearson function. The fitting range is indicated by the arrow on the abscissa. This figure is in color in the electronic version of this paper.

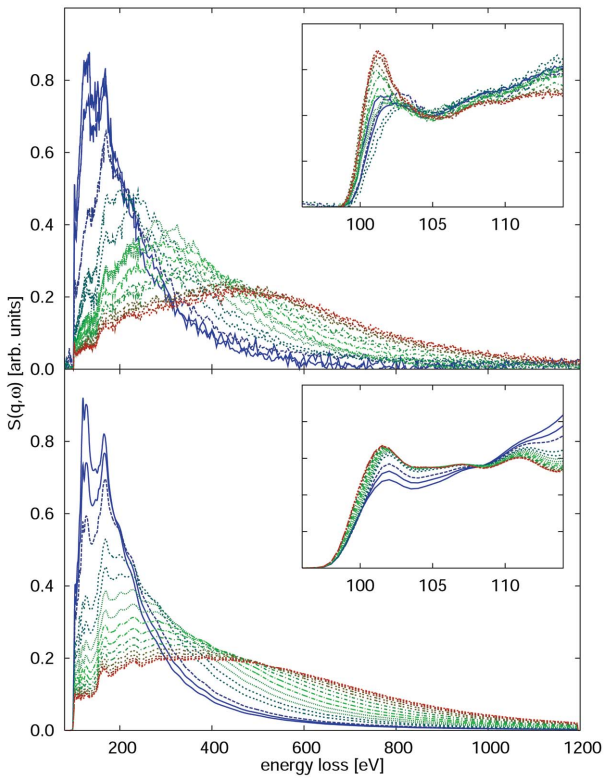

Figure 8
Top: extracted Si L edges of Si for different q. The spectra are normalized to the full area. The inset shows the near-edge region of the Si $L_{\rm II,III}$ edges normalized to the area between 95 and 110 eV. Bottom: RSMS calculations of the Si L edges in Si for the same q and with the same normalization. The wide spectra have been calculated neglecting the core hole–electron interaction while it has been accounted for in the near-edge calculations presented in the inset. This figure is in color in the electronic version of this paper.

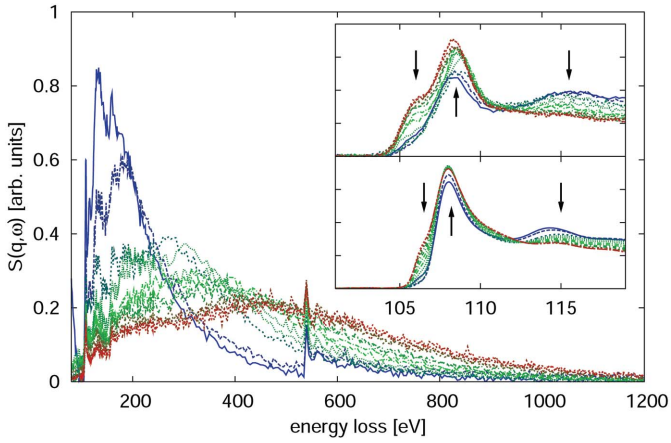

Figure 9
Extracted Si L and O K edges of SiO_2 for different q. The near-edge region is shown in the top part of the inset where the pre-edge is shifted to zero to compensate for the offset owing to the O $L_{\rm I}$ edge. The spectra are normalized to the area between 100 and 120 eV. The bottom part of the inset shows q-dependent calculations of the Si $L_{\rm II,III}$ edges employing an *ab initio* NRIXS approach based on the *StoBe-deMon* code. Corresponding features of experiment and theory are indicated by arrows. This figure is in color in the electronic version of this paper.

of $S(\mathbf{q},\omega)$ is decorated by a fine-structure. Therefore the extracted valence Compton profile only shows poor agreement in the energy region before the edge onset and the spectrum was taken out of the analysis. The resulting spectra are shown in the top part of Fig. 8 and evolve consistently for increasing momentum transfer. q-Dependent NRIXS calculations of the Si L edges have been performed employing an adaptation (Soininen *et al.*, 2005) of the real-space multiple-scattering (RSMS) code *FEFF* (Ankudinov *et al.*, 1998). The results are presented in the bottom part of Fig. 8 and show very good qualitative and quantitative agreement with the experimental spectra over the full energy range. As discussed elsewhere (Sternemann, Soininen *et al.*, 2007), the interaction of the photoelectron with the core hole is important for explaining the structure of the near-edge region whereas its neglect yields better agreement in energetic positions for higher energy losses. So, for the full range calculations without a core-hole interaction have been performed, whereas the core hole was taken into account for the near-edge region presented in the inset of Fig. 8. The broadening of the edge onset in the calculations and the absence of the peaked white line around 102 eV energy loss can be attributed to approximations used in the RSMS computation as discussed for Si by Sternemann, Soininen *et al.* (2007).

For SiO_2 the extraction is good for 14 momentum transfers. The results are shown in Fig. 9. The modulations of the O $L_{\rm I}$ edge at 41.6 eV lead to systematic errors in the Si $L_{\rm II,III}$ edges. This results in a q-dependent contribution of the NRIXS spectrum below the energy onset, whereas it should be zero for perfect subtraction as it is the case for Si. The correction of these effects is not possible within the extraction algorithm presented in this article but would require a theoretical treatment of the O $L_{\rm I}$ fine-structure. However, note that the extracted NRIXS spectra show a consistent q-dependence on the whole energy scale. Since the O $L_{\rm I}$ oscillations are assumed to be smooth very close to the absorption edge, they can be approximated by a constant offset. The top part of the inset of Fig. 9 shows the very near-edge region of the Si $L_{\rm II,III}$ edges normalized to its area. The consistency of the q-dependence can also be clearly seen here. Momentum-transfer-dependent calculations of the Si $L_{\rm II,III}$ edges have been performed employing a density functional theory *ab initio* NRIXS approach (Sakko *et al.*, 2007) based on the *StoBe-deMon* code (Hermann *et al.*, 2006). Spectra for the 14 momentum transfers were calculated for an α-quartz SiO_2 cluster of 72 atoms. Generalized gradient approximation exchange-correlation functional and triple-ζ plus valence polarization basis sets were employed. The linewidth for Lorentzian broadening was 0.1 eV below 107 eV and 2.5 eV above 110 eV with a linear increase between 107 and 110 eV energy loss. The Gaussian linewidth was 0.8 eV. The results presented in the bottom part of the inset of Fig. 9 show very good agreement with the experiment concerning the overall shape and especially the q-dependence of the features indicated by the arrows.

4. Summary and outlook

We have presented an algorithm for the subtraction of the Compton and $S(\mathbf{q},\omega)$ background from NRIXS spectra for a broad q-range. The algorithm is universal in a sense that apart from atomic Hartree–Fock core Compton profiles no sample-dependent calculations are necessary to model the background. The valence contribution to the Compton profile can be directly extracted from the experiment and used for the extraction of the edges of interest. As a proof of principle the algorithm was applied to the Si L edges in Si and SiO_2 where the extraction proved to be very successful for most of the momentum transfers. The robustness and difficulties for the extraction were discussed in detail for the different momentum transfer ranges. A comparison of q-dependent NRIXS calculations for Si and SiO_2 show the good quality of the extraction both concerning overall shape and q-dependence. Based on this study the presented algorithm yields a tool for the proper treatment of multi-q NRIXS spectra. This is of special importance for future studies, *e.g.* demanding a detailed study of the q-dependence of core excitation or an extraction of the projected density of states.

We acknowledge the Advanced Photon Source for provision of synchrotron radiation and thank Robert Gordon for assistance in using beamline XOR/PNC 20-ID. We would furthermore like to acknowledge A. Hohl for providing the Si and SiO_2 samples. We would like to thank W. Schülke and S. Huotari for useful discussions. This work was supported in part by Deutsche Forschungsgemeinschaft (Tol169/5-5), the DAAD (313-PPP-SF/06-IK), the Academy of Finland (Contract No. 111057/1112642) and the National Graduate School in Materials Physics (Finland).

References

Ankudinov, A. L., Ravel, B., Rehr, J. J. & Conradson, S. D. (1998). *Phys. Rev. B*, **58**, 7565.

Arms, D. A., Graber, T. J., Macrander, A. T., Simmons, R. O., Schwoerer-Böhning, M. & Zhong, Y. (2005). *Phys. Rev. B*, **71**, 233107.

Balasubramanian, M., Johnson, C. S., Cross, J. O., Seidler, G. T., Fister, T. T., Stern, E. A., Hammer, C. & Mariager, S. O. (2007). *Appl. Phys. Lett.* **91**, 031904.

Bergmann, U. & Cramer, S. P. (1998). *Proc. SPIE*, **3448**, 198–209.

Bergmann, U., Glatzel, P. & Cramer, S. P. (2002). *Microchem. J.* **71**, 221–230.

Bergmann, U., Nordlund, D., Wernet, Ph., Odelius, M., Pettersson, L. G. M. & Nilsson, A. (2007). *Phy. Rev. B*, **76**, 024202.

Biggs, F., Mendelsohn, L. B. & Mann, J. B. (1975). *At. Data Nucl. Data Tables*, **16**, 201–309.

Cai, Y. Q., Chow, P., Chen, C. C., Ishii, H., Tsang, K. L., Kao, C. C., Liang, K. S. & Chen, C. T. (2004). *AIP Conf. Proc.* **705**, 340–343.

Cai, Y. Q. *et al.* (2005). *Phys. Rev. Lett.* **94**, 025502.

Cooper, M. J., Mijnarends, P. E., Shiotani, N., Sakai, N. & Bansil, A. (2004). Editors. *X-ray Compton Scattering.* Oxford University Press.

Feng, Y. J., Seidler, G. T., Cross, J. O., Macrander, A. T. & Rehr, J. J. (2004). *Phys. Rev. B*, **69**, 125402.

Fister, T. T., Seidler, G. T., Hamner, C., Cross, J. O., Soininen, J. A. & Rehr, J. J. (2006). *Phys. Rev. B*, **74**, 214117.

Fister, T. T., Seidler, G. T., Wharton, L., Battle, A. R., Ellis, T. B., Cross, J. O., Macrander, A. T., Elam, W. T., Tyson, T. A. & Qian, Q. (2006). *Rev. Sci. Instrum.* **77**, 063901.

Hämäläinen, K., Galambosi, S., Soininen, J. A., Shirley, E. L., Rueff, J. P. & Shukla, A. (2002). *Phys. Rev. B*, **65**, 155111.

Hermann, K. *et al.* (2006). *StoBe-deMon*, version 2.2. http://w3.rz-berlin.mpg.de/~hermann/StoBe/index.html.

Holm, P. (1988). *Phys. Rev. A*, **37**, 3706–3719.

Holm, P. & Ribberfors, R. (1989). *Phys. Rev. A*, **40**, 6251–6259.

Hubbard, J. (1957). *Proc. R. Soc. London Ser. A*, **240**, 539–560.

Huotari, S., Hämäläinen, K., Manninen, S., Issolah, A. A. & Marangolo, M. (2001). *J. Phys. Chem. Solids*, **62**, 2205–2213.

Krisch, M. H., Sette, F., Masciovecchio, C. & Verbeni, R. (1997). *Phys. Rev. Lett.* **78**, 2843–2846.

Kumar, R. S., Cornelius, A. L., Pravica, M. G., Nicol, M. F., Hu, M. Y. & Chow, P. C. (2007). *Diamond Rel. Mater.* **16**, 1136–1139.

Lee, S. K., Eng, P. J., Mao, H. K., Meng, Y. & Shu, J. (2007). *Phys. Rev. Lett.* **98**, 105502.

Mao, W. L., Mao, H. K., Eng, P. J., Trainor, T. P., Newville, M., Kao, C. C., Heinz, D. L., Shu, J. F., Meng, Y. & Hemley, R. J. (2003). *Science*, **302**, 425–427.

Mao, W. L., Mao, H. K., Meng, Y., Eng, P. J., Hu, M. Y., Chow, P., Cai, Y. Q., Shu, J. F. & Hemley, R. J. (2006). *Science*, **314**, 636–638.

Mattila, A., Soininen, J. A., Galambosi, S., Huotari, S., Vankó, G., Zhigadlo, N. D., Karpinski, J. & Hämäläinen, K. (2005). *Phys. Rev. Lett.* **94**, 247003.

Meng, Y., Mao, H. K., Eng, P. J., Trainor, T. P., Newville, M., Hu, M. Y., Kao, C. C., Shu, J. F., Hausermann, D. & Hemley, R. J. (2004). *Nat. Mater.* **3**, 111–114.

Ribberfors, R. (1975). *Phys. Rev. B*, **12**, 2067–2074.

Sakko, A., Hakala, M., Soininen, J. A. & Hämäläinen, K. (2007). *Phys. Rev. B*, **76**, 205115.

Schülke, W. (2007). *Electron Dynamics by Inelastic X-ray Scattering.* Oxford University Press.

Soininen, J. A., Ankudinov, A. L. & Rehr, J. J. (2005). *Phys. Rev. B*, **72**, 045136.

Soininen, J. A., Mattila, A., Rehr, J. J., Galambosi, S. & Hämäläinen, K. (2006). *J. Phys. Condens. Mater.* **18**, 7327–7336.

Sternemann, C., Hämäläinen, K., Kaprolat, A., Soininen, A., Döring, G., Kao, C. C., Manninen, S. & Schülke, W. (2000). *Phys. Rev. B*, **62**, R7687–R7690.

Sternemann, C., Huotari, S., Vankó, G., Volmer, M., Monaco, G., Gusarov, A., Lustfeld, H., Sturm, K. & Schülke, W. (2005). *Phys. Rev. Lett.* **95**, 157401.

Sternemann, C., Soininen, J. A., Huotari, S., Vankó, G., Volmer, M., Secco, R. A., Tse, J. S. & Tolan, M. (2005). *Phys. Rev. B*, **72**, 035104.

Sternemann, C., Volmer, M., Soininen, J. A., Nagasawa, H., Paulus, M., Enkisch, H., Schmidt, G., Tolan, M. & Schülke, W. (2003). *Phys. Rev. B*, **68**, 035111.

Sternemann, H., Soininen, J. A., Sternemann, C., Kämäläinen, K. & Tolan, M. (2007). *Phys. Rev. B*, **75**, 075118.

Sternemann, H., Sternemann, C., Tse, J. S., Desgreniers, S., Cai, Y. Q., Vankó, G., Hiraoka, N., Schacht, A., Soininen, J. A. & Tolan, M. (2007). *Phys. Rev. B*, **75**, 245102.

Wernet, P., Nordlund, D., Bergmann, U., Cavalleri, M., Odelius, M., Ogasawara, H., Naslund, L. A., Hirsch, T. K., Ojamae, L., Glatzel, P., Pettersson, L. G. M. & Nilsson, A. (2004). *Science*, **304**, 995–999.